ACS OMEGA

http://pubs.acs.org/journal/acsodf Article

Voltage-Stabilizer-Grafted SiO_2 Increases the Breakdown Voltage of the Cycloaliphatic Epoxy Resin

Yi Qin, Shudong Zhang,* Shuai Han, Tingting Xu, Cui Liu, Min Xi, Xinling Yu, Nian Li,* and Zhenyang Wang*

Cite This: ACS Omega 2021, 6, 15523−15531 Read Online

ABSTRACT: Cycloaliphatic epoxy (CE) resin plays a vital role in insulation equipment due to its excellent insulation and processability. However, the insufficient ability of CE to confine electrons under high voltage often leads to an electric breakdown, which limits its wide applications in high-voltage insulation equipment. In this work, the interface effect of inorganic nano-SiO_2 introduces deep traps to capture electrons, which is synergistic with the inherent ability of the voltage stabilizer *m*-aminobenzoic acid (*m*-ABA) to capture high-energy electrons through collision. Therefore, the insulation failure rate is reduced owing to doping of the functionalized nanoparticles of the *m*-ABA-grafted nano-SiO_2 (*m*-ABA-SiO_2) into the CE. It is worth noting that the breakdown field strength of this *m*-ABA-SiO_2/CE reaches 53 kV/mm, which is 40.8% higher than that of pure CE. In addition, the tensile strength and volume resistivity of *m*-ABA-SiO_2/CE are increased by 29.1 and 140%, respectively. Meanwhile, the glass transition temperature was increased by about 25 °C and reached 213 °C. This work proves that the comprehensive performance of CE-based nanocomposites is effectively improved by *m*-ABA-SiO_2 nanoparticles, showing great application potential in high-voltage insulated power equipment.

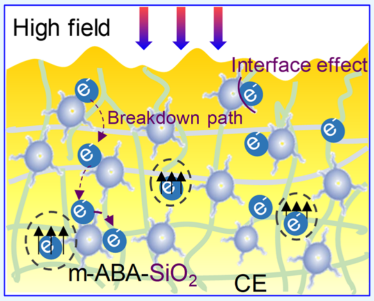

INTRODUCTION

It is well known that the safety and stability of power systems are directly affected by the insulation level of high-voltage insulation materials. Cycloaliphatic epoxy (CE) resin has excellent voltage resistance, heat resistance, and processability due to its unique structure, making it an ideal insulating material in practical applications.[1−4] According to the electrical breakdown theory of solid dielectrics, electrons are excited from the valence band to the conduction band under a sufficiently high electric field and then accelerated to collide with other atoms to generate ionized electrons.[5−7] The small current generated by the electron migration will pass through the CE, which will eventually lead to an electrical breakdown, as shown in Figure 1a. With the development of high-voltage electronic power equipment, many studies have been reported to improve the performance of insulating materials.[8−11] In fact, increasing the breakdown strength remains extremely challenging and critical in terms of reducing insulation failure rates and reliability of concern.[12−14]

So far, two kinds of important methods that have been proposed to enhance the breakdown field strength of polymers have mainly focused on the incorporation of nanofillers and voltage stabilizers.[15−18] It has been reported that the mechanism by which low content nanofillers (such as TiO_2,[19,20] MgO,[21,22] and Al_2O_3[23,24]) can improve the breakdown strength of polymer is mainly attributed to two ways: (1) the tortuous path of electron breakdown caused by nanofillers.[25,26] (2) Nanofillers capture electrons by introducing deep traps into the polymer (Figure 1b). It has been revealed that nano-SiO_2 can effectively improve the electrical insulation properties of polymers.[16,27,28] However, it is difficult for supersurficial nano-SiO_2 to disperse uniformly in the polymer, so the expected performance cannot be obtained. Therefore, it is of great importance to obtain CE-based nanocomposites with good compatibility by the surface modification of nano-SiO_2.[29] Briefly, the current urgent work is to find more effective methods to enhance the breakdown field strength of the CE-based nanocomposites.

In the past few decades, effective stabilizers have been proposed to capture high-energy electrons that would degrade polymer molecular chains through collision excitation and collision ionization (Figure 1c).[30,31] Generally, phenyl compounds with ester groups have higher electron affinity and lower ionization potential, indicating their higher ability to capture high-energy electrons.[32] Unfortunately, the stabilizer is poorly compatible with the polymer matrix and eventually loses its effectiveness due to the migration in the matrix. Therefore, it is greatly critical to improve the compatibility of the voltage stabilizer with the polymer matrix.[17] The migration

Received: April 27, 2021
Accepted: May 24, 2021
Published: May 31, 2021

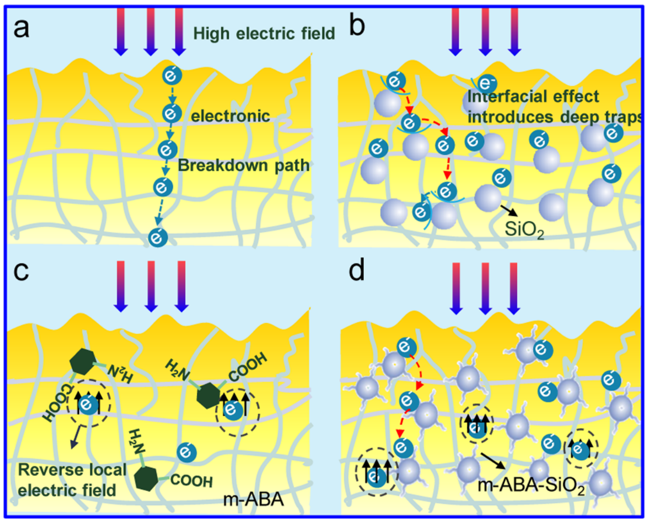

Figure 1. Diagram of the breakdown schematic of electrons on different bases. (a) Electrical breakdown schematic of pure CE; (b) electrical breakdown schematic of the SiO_2/CE nanocomposite; (c) electrical breakdown schematic of the *m*-ABA/CE composite; and (d) electrical breakdown schematic of the *m*-ABA-SiO_2/CE nanocomposite.

of the stabilizer is inhibited and the surface activity of the nanoparticles is reduced, which is expected to be realized by fixing the voltage stabilizer on the surface of the nanoparticles. There is an excellent ability for *m*-ABA to capture high-energy electrons in polymers.[33] Improving the compatibility of *m*-ABA with CE and the agglomeration of nano-SiO_2 may be achieved by grafting *m*-ABA onto nano-SiO_2 particles. This synergy makes the breakdown voltage of CE-based nanocomposites a noteworthy improvement (Figure 1d).

In this work, SiO_2-functionalized nanoparticles grafted with the *m*-ABA stabilizer were successfully added to the CE cured by anhydride. On the one hand, nano-SiO_2 is introduced into deep traps or forms scattering centers in the CE to improve the breakdown field strength. On the other hand, this strategy can improve the compatibility of *m*-ABA and CE, which is conducive to the ability of *m*-ABA to capture high-energy electrons. The cooperation between nano-SiO_2 and *m*-ABA greatly enhances the electrical breakdown performance of CE-based nanocomposites. The breakdown field strength has been increased by 40.8% to 53 kV/mm. In addition, the tensile strength and volume resistivity of *m*-ABA-SiO_2/CE are increased by 29.1% and 140%, respectively. Meanwhile, the glass transition temperature was increased by about 25 °C and reached 213 °C. It is commendable that the thermal decomposition temperature, the tensile strength, volume resistivity, and glass transition temperature T_g of CE-based nanocomposites have been enhanced by introducing the functionalized nanoparticles of the *m*-ABA-grafted nano-SiO_2 (*m*-ABA-SiO_2). The improvement of the comprehensive performance of CE-based nanocomposites makes it possible to be used in more high-voltage-resistant insulated electrical equipment.

■ RESULTS AND DISCUSSION

Structure and Morphology of the Component in the *m*-ABA-SiO_2/CE Nanocomposite. Figure 2 illustrates the process of the voltage stabilizer *m*-ABA grafted onto nano-SiO_2. First, the voltage stabilizer *m*-ABA and the aminosilane coupling agent KH-550 completed the amidation reaction at a certain temperature. Second, the siloxane group in KH-550 was hydrolyzed and bonded with Si−OH on the nano-SiO_2 to form a Si−O−Si bond. Finally, *m*-ABA-SiO_2 was obtained after washing and drying. Herein, the pristine nano-SiO_2 was observed by scanning electron microscopy (SEM) and transmission electron microscopy (TEM) (Figure S1), showing well dispersion of SiO_2 nanoparticles with a diameter of ∼18 nm. Figure S2 reveals the Fourier transform infrared (FT-IR) spectroscopy information for the grafting of *m*-ABA to nano-SiO_2. The peak at 2923 cm^{-1} is attributed to the $-CH_2-$ stretching vibration peak of the silane coupling agent KH-550. The two peaks at 1650 and 1395 cm^{-1} correspond to the stretching vibration peaks of −C═O− and −CN− after the amidation reaction, respectively. In addition, the tensile vibration peak assigned to Si−OH disappeared at 963 cm^{-1}, indicating that the dehydration reaction proceeded successfully. In summary, the functionalized particle *m*-ABA-SiO_2 was successfully prepared. Moreover, the X-ray diffraction (XRD) results are shown in Figure S3. The peak position of *m*-ABA-SiO_2 is shifted by about 1° to the right of pristine nano-SiO_2. It can be presumed to be caused by the successful grafting of *m*-ABA onto SiO_2. In addition, as shown in the thermogravimetric (TG) curve (Figure S4), the thermal weight loss of nanoparticle *m*-ABA-SiO_2 is 2 wt % more than that of pristine

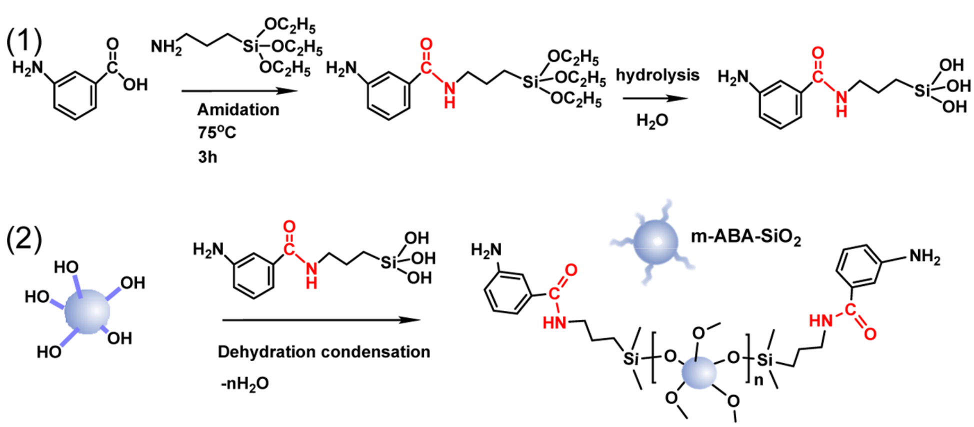

Figure 2. Diagram of the preparation mechanism of *m*-ABA-SiO_2. (1) *m*-ABA is connected to KH-550 through the amidation reaction and hydrolysis is completed. (2) Si−OH on *m*-ABA-KH-550 and SiO_2 are dehydrated and condensed to form Si−O−Si bonds to prepare *m*-ABA-SiO_2.

https://doi.org/10.1021/acsomega.1c02108
ACS Omega 2021, 6, 15523−15531

nano-SiO_2, which also confirms that *m*-ABA is successfully grafted onto SiO_2.

Regarding the curing process of the epoxy resin, first, the pre-curing temperature was kept at 100 °C for 2 h, then the temperature was increased to 150 °C for 4 h, the temperature was raised to 180 °C for 2 h, and finally, the heating was stopped and cooled to room temperature (Figure S5). In order to verify whether the CE has been completely cured, differential scanning calorimetry (DSC) test and FT-IR characterization were carried out on CE with optimized experimental conditions. As shown in Figure S6, no curing exothermic peak is observed in the DSC curve, which proves that the curing reaction has proceeded completely. In FT-IR, the tensile vibration peak of the epoxy group near 910 cm^{-1} also does not appear in Figure S7. It proves that the curing reaction of the epoxy group has proceeded completely.

During the preparation of the nanocomposite precursor fluid, we found that the amount of nanofillers is limited. When the nanoparticle-doped mass percentage is 5 wt % or less, the bubbles in the CE-based nanocomposites precursor liquid can be broken or overflow, as shown in Figure S8a−c. Above the limit of 5 wt % (relative to the total mass), the precursor solution becomes too viscous and the nanofillers cannot be better dispersed; meanwhile, a large number of bubbles cannot overflow (Figure S8d). To observe the dispersion of *m*-ABA-SiO_2 nanoparticles in CE, the cross-sectional microstructure of CE-based nanocomposites was observed by SEM. The structure of CE-based nanocomposites is very dense, as shown in Figure 3. In Figure 3a, the cross section of pure

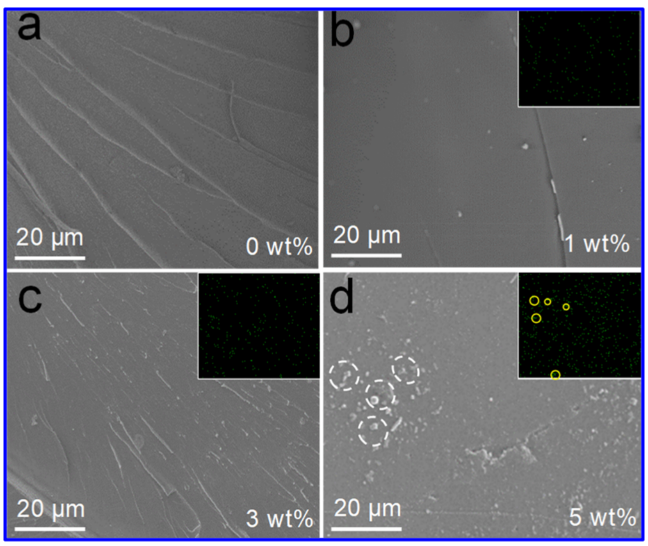

Figure 3. SEM images of the cross section of the *m*-ABA-SiO_2/CE nanocomposite material. (a−d) CE-based nanocomposites doped with (0, 1, 3, and 5 wt %) *m*-ABA-SiO_2 nanoparticles. The inset pictures (b−d) are Si element mapping in CE-based nanocomposites doped with 1, 3, and 5 wt % *m*-ABA-SiO_2 nanoparticles, respectively.

CE is free of impurities, and some fracture cracks are shown in the shiny part. It can be observed in Figure 3b that when the mass percentage of nanoparticles is 1 wt %, there is better dispersion in the CE. As the mass percentage of nanoparticles increases to 3 wt %, as shown in Figure 3c, the nanoparticles can still be dispersed well without obvious agglomeration. When the functionalized nanoparticles are continuously increased to 5 wt %, the agglomeration of nanoparticles in CE-based nanocomposites can be clearly observed in the white circled part of Figure 3d. Furthermore, when the mass percentage of nanoparticles is below 5 wt %, the measured element mapping further illustrates the uniform distribution of Si elements in CE-based nanocomposites, as shown in the inset of Figure 3b,c; when the mass percentage of nanoparticles exceeds 5 wt %, the aggregate distribution of Si in the CE-based nanocomposite material in the measured element mapping is shown by the yellow circle in the inset of Figure 3d. The reason for this phenomenon can be explained as follows: as the mass percentage of *m*-ABA-SiO_2 nanoparticles increases, the compatibility between the nanoparticles and CE becomes saturated and agglomerates.[36,37]

Thermal Stability of the *m*-ABA-SiO_2/CE Nanocomposite. Electrically insulating polymer materials often fail due to thermal degradation during actual use.[38,39] Considering the influence of temperature on the stability of the polymer structure, the thermal stability of CE-based nanocomposites was tested. The thermal decomposition curve (TG) is used to characterize the thermal weight loss of CE-based nanocomposites when the temperature rises. As shown in Figure 4a, the thermal decomposition process is divided into two

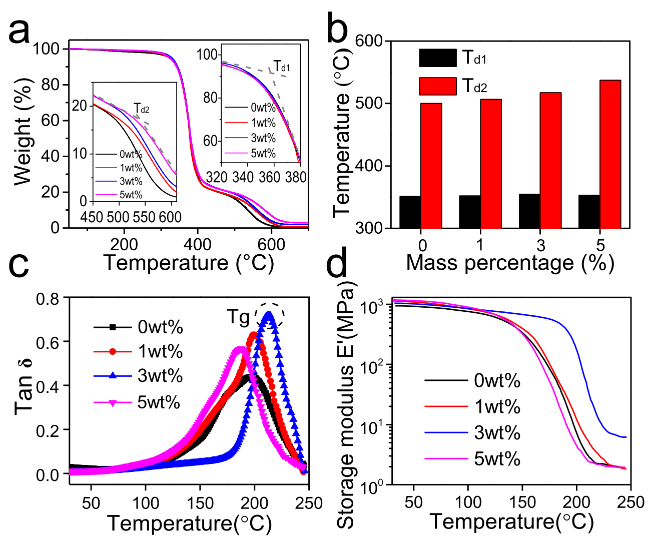

Figure 4. Effect of different mass fractions on the thermal stability of *m*-ABA-SiO_2/CE nanocomposites. (a) TG curve; (b) distribution of the decomposition temperature (T_d) histogram; (c) DMA curve; and (d) variation curve of the storage modulus between 20 and 250 °C.

steps: (1) the initial decomposition starts from some side branches of CE-based nanocomposites. The mass percentage of *m*-ABA-SiO_2 nanoparticles has almost no effect on the thermal decomposition temperature and fluctuates within 4 °C. It is worth mentioning that the CE-based nanocomposite material basically does not decompose at 350 °C. (2) As the mass percentage of *m*-ABA-SiO_2-functionalized nanoparticles increases, the decomposition temperature in the second step increases. This is due to the addition of *m*-ABA-SiO_2 nanoparticles, which produces a stronger binding force with the CE and can withstand higher temperatures. In Figure 4b, the histogram of the two-step decomposition temperature can more intuitively observe the decomposition temperature of the CE-based nanocomposite with the increase of *m*-ABA-SiO_2 nanoparticles. In short, after the addition of *m*-ABA-SiO_2 nanoparticles, the thermal decomposition temperature of the

https://doi.org/10.1021/acsomega.1c02108
ACS Omega 2021, 6, 15523−15531

CE-based nanocomposite is basically unchanged. In addition, the change trend of the decomposition temperature in the second step shows that the stability of the CE-based nanocomposites is enhanced.

Based on the correlation between the glass transition temperature (T_g) of the insulating material and the used temperature in the application, which was characterized by a dynamic thermodynamic method [dynamic mechanical analysis (DMA)]. With the addition of *m*-ABA-SiO_2 nanoparticles, the trend of T_g increases first and then decreases (Figure 4c). The T_g of CE-based nanocomposites can reach up to 213 °C at 3 wt %, which is an increase of 25 °C compared with that of pure CE. When the mass percentage of *m*-ABA-SiO_2 nanoparticles is increased to 5 wt %, the excessive nanoparticles have poor dispersion in the CE-based nanocomposites, resulting in a decrease about T_g. After the temperature exceeds T_g, the physical properties of CE-based nanocomposites (such as mechanical properties and insulation properties) will be damaged.[40] Correspondingly, the increase in T_g also indicates that the structure of the nanocomposite is more stable.

The rigidity of CE-based nanocomposites can be characterized by the storage modulus (E'). Figure 4d shows that when a certain temperature is reached, the E' of the *m*-ABA-SiO_2/CE nanocomposite material drops rapidly by 3 orders of magnitude, which means that the rigidity of the material is reduced rapidly. As the mass percentage of *m*-ABA-SiO_2 increases, the transition temperature of the CE-based nanocomposite E' is increased, which is beneficial to enhance the heat resistance of the material under alternating stress. When increased to 3 wt %, the transition temperature is the highest (~210 °C). When the nanoparticles continue to increase to 5 wt %, defects are introduced due to nanoparticle agglomeration in the CE-based nanocomposites, resulting in a decrease in the transition temperature of E'. Due to the excellent dispersion of *m*-ABA-SiO_2 nanoparticles in the CE, the force between the molecular chains is increased and the CE structure is more stable.[41] By the way, this trend is consistent with the change of T_g with the increase of *m*-ABA-SiO_2 nanoparticles.

Mechanical Properties of the *m*-ABA-SiO_2/CE Nanocomposite. In order to determine the internal structural reliability of CE-based nanocomposites, tensile performance tests were used to characterize the structural stability of CE-based nanocomposites.[42] Figure 5 shows the tensile strength test results of the *m*-ABA-SiO_2/CE nanocomposite. As shown in Figure 5a, with the increase of the *m*-ABA-SiO_2 content, the change trend of the tensile strength is to increase first and then decrease. When the content is 3 wt %, the maximum tensile strength is 86.43 MPa, which is 29.1% stronger than pure CE. The bar graph (Figure 5b) shows the tensile strength distribution of the *m*-ABA-SiO_2/CE nanocomposite tested multiple times. It can be explained that the addition of *m*-ABA-SiO_2 nanoparticles will improve the density of crosslinking points of polymer molecular chains and increase the cohesive energy of the molecules, thereby making the entire structure more compact and difficult to destroy.[43,44] Due to the continuous increase of *m*-ABA-SiO_2 nanoparticles, they cannot be well dispersed in CE-based nanocomposite materials. The agglomerated part introduces physical defects and hinders the entanglement between molecular chains, thereby increasing the local free volume and reducing its tensile properties.[45]

As shown in Figure 5c, with the increase of *m*-ABA-SiO_2 nanoparticles, the Young's modulus also shows a certain regularity. When the content is 3 wt %, the maximum value is 2.65 GPa, which is 44.8% higher than pure CE. When the *m*-ABA-SiO_2 nanoparticles increase to 5 wt %, the Young's modulus shows a decreasing trend. The results show that when the mass percentage of *m*-ABA-SiO_2 nanoparticles is 3 wt %, the CE-based nanocomposite has good compatibility and high cohesive energy. Based on the split strength model, the theoretical breakdown strength is positively correlated with the cohesive energy.[5] The higher Young's modulus means that the nanocomposite material can withstand the higher Coulomb force generated by the external electric field.[46,47] In other words, the *m*-ABA-SiO_2 nanoparticles in the CE-based nanocomposites may form strong physical support points to protect the nanocomposite from electromechanical failure. In Figure 5d, it is observed that pure CE is brittle under external force. On the contrary, after doping with *m*-ABA-SiO_2, the brittleness of the CE-based nanocomposite is improved, and a certain degree of bending deformation can occur under external force, as shown in Figure 5e. Regarding the processing performance, while the tensile strength is improved, it can still be processed into different shapes. In Figure S9, it can be observed that the CE-based nanocomposite exhibits excellent processing performance, which is beneficial to a wider range of applications.

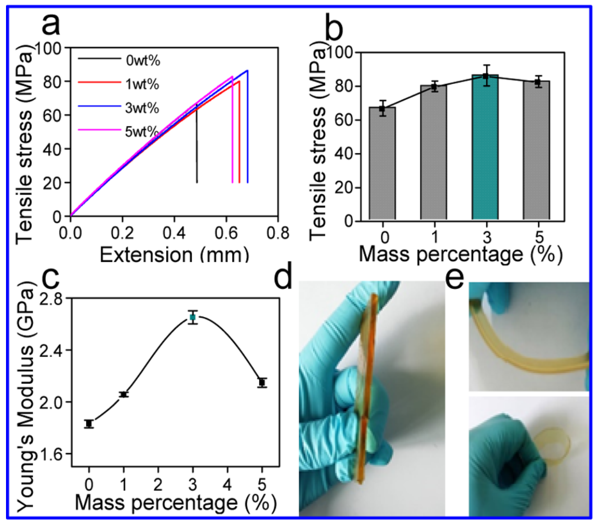

Figure 5. Influence of different mass fractions on the mechanical properties of *m*-ABA-SiO_2/CE nanocomposites. (a) Stress−strain curve; (b) distribution of the tensile strength histogram; (c) Young's modulus curve; (d) brittleness of pure CE; and (e) *m*-ABA-SiO_2/CE nanocomposite material's certain flexibility.

Electrical Insulation Properties of the *m*-ABA-SiO_2/CE Nanocomposite. High resistivity is very important for the application of CE-based nanocomposites to high-voltage insulation equipment.[48] Therefore, the volume resistivity of *m*-ABA-SiO_2/CE nanocomposites with different mass percentages was measured to evaluate the insulation properties of CE-based nanocomposites. As shown in Figure 6, as the mass percentage of *m*-ABA-SiO_2 increases, the volume resistivity changes first to increase and then to decrease. The maximum value obtained at 3 wt % is 5.47×10^{14} Ω·m, which is 2.4 times that of pure CE. The gain of volume resistivity can be mainly attributed to two ways: (1) the dispersion of *m*-ABA-SiO_2 nanoparticles in CE serves as a physical obstacle to cause the tortuous path of electron migration.[25] (2) The electrons are trapped in the interface traps introduced by the *m*-ABA-SiO_2-

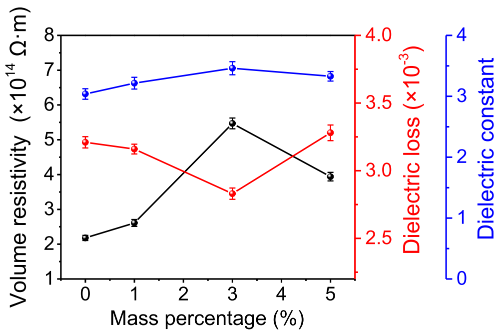

Figure 6. Volume resistivity (black line), dielectric constant (blue line), and dielectric loss (red line) of *m*-ABA-SiO_2/CE nanocomposites with different mass percentages.

functionalized nanoparticles with CE.[27] At this time, a higher voltage is required for the electrons to escape from the traps of the nanocomposite. The combined effect of the two effects greatly increases the volume resistivity of the nanocomposite. Such a high resistivity or low electrical conductivity indicates that the Joule heat generated by the CE-based nanocomposite is extremely low, which is beneficial to avoid thermoelectric breakdown.[49,50]

Joule heat generated by the leakage current of the insulating material becomes the main cause of the dielectric loss. The current flowing through the polymer converts a part of the electronic kinetic energy into Joule heat, which is closely related to the volume resistivity. As shown in Figure 6, the dielectric loss has a negative correlation with the change trend of volume resistivity. The larger the volume resistivity of the CE-based nanocomposite, the smaller the corresponding leakage current that can flow through the matrix and the relatively low dielectric loss. When the mass percentage of *m*-ABA-SiO_2 is 3 wt %, the minimum dielectric loss is 0.0028, which is 12% lower than that of the pure CE. In short, the dielectric loss is kept at a very low value, which is conducive to the insulation performance of CE-based nanocomposites.[48]

As shown in Table S1, compared with other nanofillers such as TiO_2, MgO, and Al_2O_3, the dielectric constant of SiO_2 is 3.9, so it has a higher dielectric match rate with the pure CE (the dielectric constant value is about 3.0). Figure 6 shows that when the mass percentage of *m*-ABA-SiO_2 nanoparticles is 3 wt %, the dielectric constant of the CE reaches the maximum of 3.5. This can be attributed to the fact that the dielectric constant of silicon dioxide is slightly larger than that of the host matrix in the first place. In addition, the mass percentage of *m*-ABA-SiO_2 increases and the specific surface area increases, resulting in an increase in the interface and polarization. When the dispersion of *m*-ABA-SiO_2 nanoparticles in CE continues to increase to 5 wt %, the dielectric constant has a downward trend. According to the mechanism of the potential barrier model, the difference in interface characteristics and the content of nanofillers leads to a decrease of the dielectric constant, and its changing trend model is similar to the reported polymer-based nanocomposites in literature studies.[51−53]

When the filler is at the nanolevel, the dielectric properties are mainly affected by the interface effect.[54,55] The increase in dielectric constant indicates that the addition of *m*-ABA-SiO_2 nanoparticles introduces more interface effects. It has been proved that the interfacial interaction between nanoparticles and the CE can effectively increase the breakdown voltage of the CE. Figure S10 shows the Weibull distribution of the measured breakdown strengths of KH-550-SiO_2/CE (KH-550 silane coupling agent-modified nano-SiO_2). It can be observed that when the modified nano-SiO_2 mass percentage is 3 wt %, the maximum value of 47 kV/mm is obtained, which is an increase of 24.8% compared to that of pure CE. It reveals that nano-silica plays a positive role in the increase of CE-based nanocomposites' breakdown field strength.

Then, the voltage stabilizer *m*-ABA silane coupling agent is fixed on the SiO_2 nanoparticles by KH-550 to prepare *m*-ABA-SiO_2-functionalized nanoparticles, which are doped into CE. It was found that compared with the KH-550-SiO_2/CE nanocomposite, the breakdown voltage of the *m*-ABA-SiO_2/CE nanocomposite was further improved to 53 kV/mm, which is 40.8% higher than that of pure CE, as shown in Figure 7.

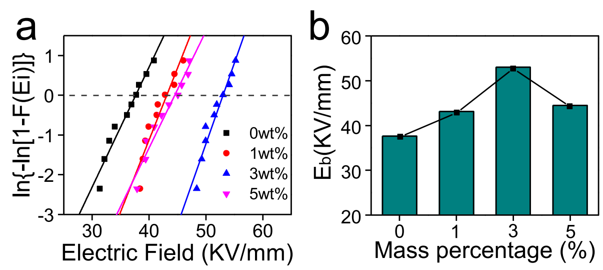

Figure 7. Electrical breakdown performance of *m*-ABA-SiO_2/CE nanocomposites. (a) Weibull distribution of measured breakdown strengths of nanocomposites. The solid lines refer to the fitting results using a two-parameter Weibull distribution function (see the Experimental Section). (b) Effect of *m*-ABA-SiO_2 with different mass percentages on CE-based nanocomposites' breakdown field strength (E_b).

When the content of nanoparticles reaches 5 wt %, the electrical breakdown strength decreases. The addition of excessive nanoparticles will result in a decrease in the breakdown strength because they will agglomerate in the CE-based nanocomposites and introduce more defects, destroying the basic structure of CE. This proves that after the voltage stabilizer is fixed on the surface of nano-SiO_2, it can play an active role in increasing the breakdown voltage. In Table S2, the breakdown strength enhancement mentioned in this work and the report are compared. It can be seen that when the dispersing filler is SiO_2 nanoparticles, compared with other surface modifiers, the gain of the voltage stabilizer *m*-ABA on the breakdown strength of the matrix is at a higher level. In summary, compared with the reported nanocomposite materials, *m*-ABA-SiO_2 exhibits a higher CE breakdown strength enhancement. This proves that *m*-ABA has a positive effect on the improvement of the CE breakdown field strength.

The increase in the breakdown voltage of CE-based nanocomposites can be attributed to the collective synergistic effect of SiO_2 nanoparticles and voltage stabilizer *m*-ABA. The smaller size effect of *m*-ABA-SiO_2 nanoparticles forms a special interface with the CE, thereby introducing deep traps in the CE.[56−58] The electrons are trapped in deep traps, weakening the kinetic energy, thereby reducing the possibility of breakdown.[59,60] Figure S11 shows the results of the thermally stimulated depolarization current (TSDC) of the *m*-ABA-SiO_2/CE nanocomposite. The temperature and intensity of the TSDC peak can be correlated with the depth and density of the charge traps, respectively. It can be observed that the *m*-ABA-SiO_2/CE nanocomposite has a TSDC peak at a higher temperature (above 125 °C), which corresponds to a higher trap depth. It can be inferred that the composite material has a lower charge mobility. In addition, the temperature around 95 °C corresponds to a shallower trap depth, and the peak of the *m*-ABA-SiO_2/CE nanocomposite is not obvious here, which means that the shallow trap density is reduced. As the mass percentage of *m*-ABA-SiO_2 nanoparticles increases, the current intensity (corresponding to the trap density) first increases and then decreases, which also affects the migration of carriers. This result is consistent with the characterized volume resistivity and voltage breakdown strength results (Figure S11). It proves that the CE doped with *m*-ABA-SiO_2 nanoparticles does introduce deep traps to reduce the migration of carriers and improve the CE electrical breakdown performance to a certain extent. The successful introduction of *m*-ABA-SiO_2 nanoparticles provides an effective method for increasing the breakdown field strength of high-voltage insulation materials.

■ CONCLUSIONS

In summary, we have developed a method of grafting stabilizers onto nano-SiO_2 using the collective synergistic to improve the electrical breakdown strength of CE-based nanocomposites. *m*-ABA-SiO_2 was dispersed uniformly in the CE matrix, and the molecular chains were cross-linked through a gradual curing process to prepare CE-based nanocomposite materials with high-voltage breakdown resistance, excellent thermal stability, good tensile strength, and easy-to-process. The prepared CE-based nanocomposite material does not decompose at 350 °C and can still maintain a stable structure at 200 °C; the tensile strength can reach 86 MPa, and it has a certain degree of toughness. What is more, the breakdown electric field strength can reach 53 kV/mm, which is an increase of 40.8% compared with that of pure CE. The introduction of *m*-ABA-SiO_2-functionalized nanoparticles can effectively increase the breakdown field strength of CE-based nanocomposites, which provides new opportunities for the reliable insulation of high-voltage electronic power equipment.

■ EXPERIMENTAL SECTION

Prepared Raw Materials. 3,4-Epoxycyclohexylmethyl-3,4-epoxycyclohexanecarboxylate (CE, epoxy value of 0.74−0.80), methyl-5-norbornene-2,3-dicarboxylic anhydride (MNA, 95%) was used as the hardener, and tris(dimethylaminomethyl)-phenol (DMP-30, 95%) was used as the accelerator. Fumed nano-SiO_2 (20 nm, 99%) was purchased from Aladdin Reagent. γ-Aminopropyl triethoxysilane (KH-550, 99%) and analytical-grade toluene and *m*-aminobenzoic acid (*m*-ABA, 99%) were provided by Sinopharm Chemical Reagent.

Synthesis of *m*-ABA-Grafted Nano-SiO_2. First, stoichiometric amounts of KH-550 and *m*-ABA are used to prepare aminosilane-modified *m*-ABA through a liquid-phase reaction. 0.01 mol *m*-ABA was taken and stirred in 20 mL of toluene solution. After complete dissolution, 0.01 mol KH-550 was added dropwise to the mixed solution and stirred at 75 °C for 3 h to complete the amidation reaction. Next, the nano-SiO_2 particles were dispersed in toluene and added to the above solution. Finally, 2 mL of water was added dropwise and stirred overnight at 75 °C. The obtained product was repeatedly washed with ethanol and water and then dried at 60 °C. This method produced *m*-ABA-grafted nano-SiO_2, namely, *m*-ABA-SiO_2.

Synthesis of CE. The mass ratio of CE to MNA is set to 1:1.2; the dosage of DMP-30 is 5 wt % of the mass of CE.[34] Then, the three liquids are uniformly mixed in proportion by mechanical stirring and ultrasound. After vacuuming, the mixed precursor solution is cast on a mold preheated to 100 °C and the temperature is gradually increased. First, it was heated at 100 °C for 2 h, then heated to 150 °C for 4 h, and then heated at 180 °C for 2 h[35] Finally, the sample was obtained after being cooled to room temperature.

Preparation of *m*-ABA-SiO_2/CE Nanocomposites. For CE nanocomposites, different mass percentages (0, 1, 3, and 5 wt %) of *m*-ABA-SiO_2 were added into CE by stirring and sonicating to form a homogeneous suspension at room temperature. Then, MNA and DMP-30 were added to the suspension. Then, MNA and DMP-30 were added to the suspension in turn. After vacuuming, the suspension was cast onto the mold and cured by a temperature program. For comparison, the KH-550 silane-modified SiO_2/CE nanocomposite with the corresponding same filling amount was fabricated as the control following the same steps as above.

Characterization. Nanoparticles, CE, and nanocomposite materials were measured by using FT-IR spectrometry (Nicolet 8700) to provide enough information about functional groups. The surface morphology was observed using a scanning electron microscope (Gemini SEM 500, Carl Zeiss Microscopy Ltd.). The morphology and corresponding energy-dispersive X-ray spectroscopy (EDS) elemental mapping images of CE-based nanocomposites were measured by SEM. The morphology of nanoparticles was characterized by TEM (JEOL JEM-ARM200F). For TEM measurement, nano-SiO_2 was dispersed in an ethanol solution separately. One drop of the dispersion solution was dropped on an ultrathin copper mesh to guarantee a fine contrast between the background. A differential scanning calorimeter (DSC Q2000) was used to control the curing conditions and determine the reaction conditions for complete curing. The thermal decomposition temperature can be obtained by TG curves. The TG curves of CE-based nanocomposites were measured by a synchronous thermal analyzer (SDT650), and the temperature is increased from 20 to 800 °C at a heating rate of 10 °C/min. The DMA test was performed by an analyzer DMA Q800. For DMA measurement, the nanocomposite samples were heated and cooled between 30 and 250 °C at a temperature change rate of 5 °C/min. The tensile strength is characterized by the Instron9657 multifunctional electronic universal material mechanical property testing machine, which is stretched at a rate of 2 mm/min at room temperature. According to the GB/T1408.1-2016 test standard, a breakdown test platform for epoxy resin cured samples was built. The adjustable range of the power frequency voltage amplitude of the test transformer is 0−50 kV. The electrode adopts a ball−ball electrode, which is made of stainless steel with two identical ball electrodes with a diameter of 20 mm. The characteristic breakdown strengths of nanocomposites can be described by a two-parameter Weibull distribution function, as follows

$$F(E_i) = 1 - \exp\left[-\left(\frac{E_i}{E_b}\right)^{\beta}\right] \tag{1}$$

where $F(E_i)$ is the failure probability when the breakdown voltage is less than or equal to E_i and β is the Weibull modulus for evaluating the distribution width. E_i is the measured breakdown strength each time and is sorted from the smallest to the largest. At the same time, E_b and β are fit parameters. The fit parameters can be extracted by linearizing eq 1

$$\ln\left[\ln \frac{1}{1 - F(E_i)}\right] = \beta \ln E_i - \beta \ln E_b \tag{2}$$

The volume resistivity of epoxy-based nanocomposites was measured by Keithley6517 at room temperature. The dielectric constant and loss tangent were measured by an LCR meter (Agilent 4294A) with a 0.5 V AC signal in 50 Hz. The density and depth of traps in nanocomposites are characterized by TSDC. First, the sample is heated to 70 °C, and then, a DC electric field (3 kV/mm) is applied under isothermal conditions for 20 min. Then, the sample was cooled to −50 °C, while the electric field is still on. Finally, while measuring the depolarization current with an ammeter, the sample was short-circuited and linearly heated to 180 °C at 3 °C/min. In order to ensure the reproducibility of the experimental results, it was confirmed that the material preparation process was carried out under the same conditions. For nanocomposites with different mass percentages, at least three different samples should be prepared for all tests.

■ ASSOCIATED CONTENT

Supporting Information

The Supporting Information is available free of charge at https://pubs.acs.org/doi/10.1021/acsomega.1c02108.

> Characterization of the microscopic morphology of nano-SiO_2, surface group changes of nano-SiO_2 measured by FT-IR before and after grafting *m*-ABA, XRD and TG results of SiO_2 and *m*-ABA-SiO_2, respectively, preparation process of the *m*-ABA-SiO_2/CE nanocomposite, DSC curve and FT-IR spectrum of pure CE cured, processability of the CE-based nanocomposite, dielectric constants of several samples, electrical breakdown performance of KH-550-modified SiO_2/CE nanocomposites, and summary of the E_b and T_g of the polymer matrix described in some papers (PDF)

■ AUTHOR INFORMATION

Corresponding Authors

Shudong Zhang − *Institute of Solid State Physics, Hefei Institutes of Physical Science, Chinese Academy of Sciences, Hefei, Anhui 230031, China; Key Laboratory of Photovoltaic and Energy Conservation Materials, Hefei Institutes of Physical Science, Chinese Academy of Sciences, Hefei 230031, China;* orcid.org/0000-0002-0215-1641; Email: sdzhang@iim.ac.cn

Nian Li − *Institute of Solid State Physics, Hefei Institutes of Physical Science, Chinese Academy of Sciences, Hefei, Anhui 230031, China; Key Laboratory of Photovoltaic and Energy Conservation Materials, Hefei Institutes of Physical Science, Chinese Academy of Sciences, Hefei 230031, China;* Email: linian@issp.ac.cn

Zhenyang Wang − *Institute of Solid State Physics, Hefei Institutes of Physical Science, Chinese Academy of Sciences, Hefei, Anhui 230031, China; Key Laboratory of Photovoltaic and Energy Conservation Materials, Hefei Institutes of Physical Science, Chinese Academy of Sciences, Hefei 230031, China;* orcid.org/0000-0002-0194-3786; Email: zywang@iim.ac.cn

Authors

Yi Qin − *Institute of Solid State Physics, Hefei Institutes of Physical Science, Chinese Academy of Sciences, Hefei, Anhui 230031, China; Department of Chemistry, University of Science and Technology of China, Hefei 230026, China*

Shuai Han − *Institute of Solid State Physics, Hefei Institutes of Physical Science, Chinese Academy of Sciences, Hefei, Anhui 230031, China; Department of Chemistry, University of Science and Technology of China, Hefei 230026, China*

Tingting Xu − *Institute of Solid State Physics, Hefei Institutes of Physical Science, Chinese Academy of Sciences, Hefei, Anhui 230031, China; Department of Chemistry, University of Science and Technology of China, Hefei 230026, China*

Cui Liu − *Institute of Solid State Physics, Hefei Institutes of Physical Science, Chinese Academy of Sciences, Hefei, Anhui 230031, China; Key Laboratory of Photovoltaic and Energy Conservation Materials, Hefei Institutes of Physical Science, Chinese Academy of Sciences, Hefei 230031, China*

Min Xi − *Institute of Solid State Physics, Hefei Institutes of Physical Science, Chinese Academy of Sciences, Hefei, Anhui 230031, China; Key Laboratory of Photovoltaic and Energy Conservation Materials, Hefei Institutes of Physical Science, Chinese Academy of Sciences, Hefei 230031, China*

Xinling Yu − *Institute of Solid State Physics, Hefei Institutes of Physical Science, Chinese Academy of Sciences, Hefei, Anhui 230031, China; Key Laboratory of Photovoltaic and Energy Conservation Materials, Hefei Institutes of Physical Science, Chinese Academy of Sciences, Hefei 230031, China*

Complete contact information is available at: https://pubs.acs.org/10.1021/acsomega.1c02108

Notes

The authors declare no competing financial interest.

■ ACKNOWLEDGMENTS

We appreciate the support of the National Key Research and Development Project (SQ2020YFA020050-03), the Science and Technology Service Network Initiative of Chinese Academy of China (grant KFJ-STS-ZDTP-080), the National Natural Science Foundation of China (nos. U2032158, U2032159, and 62005292), the Collaborative Innovation Program of Hefei Science Center, CAS (2020HSC-CIP003), the Major Scientific and the CASHIPS Director's Fund (YZJJZX202015), the Key Research and Development Program of Anhui Province (201904a05020009), and the Technological Innovation Projects of Shandong Province (2019JZZY020243).

■ REFERENCES

(1) Liu, W.; Wang, Z.; Xiong, L.; Zhao, L. Phosphorus-containing liquid cycloaliphatic epoxy resins for reworkable environment-friendly electronic packaging materials. *Polymer* **2010**, *51*, 4776−4783.

(2) Chao, P.; Li, Y.; Gu, X.; Han, D.; Jia, X.; Wang, M.; Zhou, T.; Wang, T. Novel phosphorus-nitrogen-silicon flame retardants and their application in cycloaliphatic epoxy systems. *Polym. Chem.* **2015**, *6*, 2977−2985.

(3) Gao, N.; Liu, W.; Yan, Z.; Wang, Z. Synthesis and properties of transparent cycloaliphatic epoxy-silicone resins for opto-electronic devices packaging. *Opt. Mater.* **2013**, *35*, 567−575.

(4) Sangermano, M.; Deorsola, F.; Fabiani, D.; Montanari, G.; Rizza, G. Epoxy-boehmite nanocomposites as new insulating materials. *J. Appl. Polym. Sci.* **2009**, *114*, 2541−2546.

(5) Bao, Z.; Hou, C.; Shen, Z.; Sun, H.; Zhang, G.; Luo, Z.; Dai, Z.; Wang, C.; Chen, X.; Li, L.; Yin, Y.; Shen, Y.; Li, X. Negatively charged

nanosheets significantly enhance the energy-storage capability of polymer-based nanocomposites. *Adv. Mater.* **2020**, *32*, 1907227.

(6) Chen, H.; Chen, X.; Shi, J.; Sun, C.; Dong, X.; Pang, F.; Zhou, H. Achieving ultrahigh energy storage density in $NaNbO_3$-Bi-$(Ni_{0.5}Zr_{0.5})O_3$ solid solution by enhancing the breakdown electric field. *Ceram. Int.* **2020**, *46*, 28407−28413.

(7) Hu, B.; Fan, H.; Ning, L.; Wen, Y.; Wang, C. High energy storage performance of $[(Bi_{0.5}Na_{0.5})_{0.94}Ba_{0.06}]_{0.97}La_{0.03}Ti_{1-x}(Al_{0.5}Nb_{0.5})_xO_3$ ceramics with enhanced dielectric breakdown strength. *Ceram. Int.* **2018**, *44*, 15160−15166.

(8) Cui, H.; Zhang, X.; Zhang, J.; Zhang, Y. Nanomaterials-based gas sensors of SF_6 decomposed species for evaluating the operation status of high-voltage insulation devices. *High Volt.* **2019**, *4*, 242−258.

(9) Li, P.; Hong, Q.; Wu, T.; Cui, H. SOF_2 sensing by Rh-doped PtS_2 monolayer for early diagnosis of partial discharge in the SF_6 insulation device. *Mol. Phys.* **2021**, No. e1919774.

(10) Zhang, X.; Chen, Z.; Chen, D.; Cui, H. Adsorption behaviour of SO_2 and SOF_2 gas on Rh-doped BNNT: a DFT study. *Mol. Phys.* **2020**, *118*, No. e1580394.

(11) Cui, H.; Zhang, X.; Zhang, J.; Tang, J. Adsorption behaviour of SF_6 decomposed species onto Pd_4-decorated single-walled CNT: a DFT study. *Mol. Phys.* **2018**, *116*, 1749−1755.

(12) Andraschek, N.; Wanner, A. J.; Ebner, C.; Riess, G. Mica/epoxy-composites in the electrical industry: applications, composites for insulation, and investigations on failure mechanisms for prospective optimizations. *Polymers* **2016**, *8*, 201.

(13) He, J.; Wang, H.; Qu, Q.; Su, Z.; Qin, T.; Tian, X. Three-dimensional network constructed by vertically oriented multilayer graphene and SiC nanowires for improving thermal conductivity and operating safety of epoxy composites with ultralow loading. *Composites, Part A* **2020**, *139*, 106062.

(14) Tao, Z.; Yang, S.; Chen, J.; Fan, L. Synthesis and characterization of imide ring and siloxane-containing cycloaliphatic epoxy resins. *Eur. Polym. J.* **2007**, *43*, 1470−1479.

(15) Su, J.; Du, B.; Han, T.; Li, J.; Li, Z.; Xiao, M. Nanoscale-trap-modulated electrical degradation in polymer dielectric composites using antioxidants as voltage stabilizers. *Composites, Part B* **2019**, *178*, 107434.

(16) Abdel-Gawad, N. M. K.; El Dein, A. Z.; Mansour, D.-E. A.; Ahmed, H. M.; Darwish, M. M. F.; Lehtonen, M. Multiple enhancement of PVC cable insulation using functionalized SiO_2 nanoparticles based nanocomposites. *Electr. Power Syst. Res.* **2018**, *163*, 612−625.

(17) Li, X.; Guo, Q.; Sun, X.; Yang, F.; Li, W.; Yao, Z. Effective strategy for improving the dielectric strength and insulation lifetime of LLDPE. *Ind. Eng. Chem. Res.* **2019**, *58*, 9372−9379.

(18) Nilagiri Balasubramanian, K. B.; Ramesh, T. Role, effect, and influences of micro and nano-fillers on various properties of polymer matrix composites for microelectronics: A review. *Polym. Adv. Technol.* **2018**, *29*, 1568−1585.

(19) Abdel-Gawad, N. M. K.; El Dein, A. Z.; Mansour, D.-E. A.; Ahmed, H. M.; Darwish, M. M. F.; Lehtonen, M. Enhancement of dielectric and mechanical properties of polyvinyl chloride nanocomposites using functionalized TiO_2 nanoparticles. *IEEE Trans. Dielectr. Electr. Insul.* **2017**, *24*, 3490−3499.

(20) Tse, M.-Y.; Wei, X.; Wong, C.-M.; Huang, L.-B.; Lam, K.-h.; Dai, J.; Hao, J. Enhanced dielectric properties of colossal permittivity co-doped TiO_2/polymer composite films. *RSC Adv.* **2018**, *8*, 32972−32978.

(21) Cheng, Q.; Zha, J.-W.; Zhai, J.-T.; Zhang, D.-L.; Bian, X.; Chen, G.; Dang, Z.-M. Improved space charge suppression in PP/SEBS nanocomposites by controlling MgO nanoparticles with abundant surface defects. *Appl. Phys. Lett.* **2019**, *115*, 102904.

(22) Li, Z.; Cao, W.; Sheng, G.; Jiang, X.; Danikas, M. G. Experimental study on space charge and electrical strength of MgO nano-particles/polypropylene composite. *IEEE Trans. Dielectr. Electr. Insul.* **2016**, *23*, 1812−1819.

(23) Wang, S.; Chen, Y.; Mao, J.; Liu, C.; Zhang, L.; Cheng, Y.; Du, C.; Tanaka, T. Dielectric strength of glass fibre fabric reinforced epoxy by nano-Al_2O_3. *IEEE Trans. Dielectr. Electr. Insul.* **2020**, *27*, 1086−1094.

(24) Yang, X.; Jiang, Z.; Li, W.; Wang, C.; Chen, M.; Zhang, G. The role of interfacial H-bonding on the electrical properties of UV-cured resin filled with hydroxylated Al_2O_3 nanoparticles. *Nanotechnology* **2020**, *31*, 275710.

(25) Zeng, Y.; Shen, Z.-H.; Shen, Y.; Lin, Y.; Nan, C.-W. High energy density and efficiency achieved in nanocomposite film capacitors via structure modulation. *Appl. Phys. Lett.* **2018**, *112*, 103902.

(26) Dai, C.; Chen, X.; Jiang, T.; Paramane, A.; Tanaka, Y. Improvement of electrical and material properties of epoxy resin/aluminum nitride nanocomposites for packaging materials. *Polym. Test.* **2020**, *86*, 106502.

(27) Zhang, L.; Khani, M. M.; Krentz, T. M.; Huang, Y. H.; Zhou, Y. X.; Benicewicz, B. C.; Nelson, J. K.; Schadler, L. S. Suppression of space charge in crosslinked polyethylene filled with poly(stearyl methacrylate)-grafted SiO_2 nanoparticles. *Appl. Phys. Lett.* **2017**, *110*, 132903.

(28) Chen, Q.; Yang, H.; Wang, X.; Liu, H.; Zhou, K.; Ning, X. Dielectric properties of epoxy resin impregnated nano-sio_2 modified insulating paper. *Polymers* **2019**, *11*, 393.

(29) Shi, H.; Liu, F.; Yang, L.; Han, E. Characterization of protective performance of epoxy reinforced with nanometer-sized TiO_2 and SiO_2. *Prog. Org. Coat.* **2008**, *62*, 359−368.

(30) Jarvid, M.; Johansson, A.; Kroon, R.; Bjuggren, J. M.; Wutzel, H.; Englund, V.; Gubanski, S.; Andersson, M. R.; Müller, C. A new application area for fullerenes: voltage stabilizers for power cable insulation. *Adv. Mater.* **2015**, *27*, 897−902.

(31) Gao, Y.; Huang, X.; Min, D.; Li, S.; Jiang, P. Recyclable Dielectric Polymer nanocomposites with voltage stabilizer interface: toward new generation of high voltage direct current cable insulation. *ACS Sustainable Chem. Eng.* **2019**, *7*, 513−525.

(32) Jarvid, M.; Johansson, A.; Englund, V.; Lundin, A.; Gubanski, S.; Müller, C.; Andersson, M. R. High electron affinity: a guiding criterion for voltage stabilizer design. *J. Mater. Chem. A* **2015**, *3*, 7273−7286.

(33) Chen, X.; Yu, L.; Dai, C.; Paramane, A.; Liu, H.; Wei, Z.; Tanaka, Y. Enhancement of insulating properties of polyethylene blends by delocalization type voltage stabilizers. *IEEE Trans. Dielectr. Electr. Insul.* **2019**, *26*, 2041−2049.

(34) Monte, D.; Galià, M.; Cádiz, V.; Mantecón, A.; Serra, A. Synthesis and crosslinking of new bis(4,5-epoxytetrahydrophthalimides). *Macromol. Chem. Phys.* **1995**, *196*, 1051−1061.

(35) Fu, K.; Xie, Q.; Lü, F.; Duan, Q.; Wang, X.; Zhu, Q.; Huang, Z. Molecular dynamics simulation and experimental studies on the thermomechanical properties of epoxy resin with different anhydride curing agents. *Polymers* **2019**, *11*, 975.

(36) Zheng, J.; Zhang, X.; Cao, J.; Chen, R.; Aziz, T.; Fan, H.; Bittencourt, C. Behavior of epoxy resin filled with nano-SiO 2 treated with a Eugenol epoxy silane. *J. Appl. Polym. Sci.* **2020**, *138*, 50138.

(37) Wang, M.; Ma, L.; Shi, L.; Feng, P.; Wang, X.; Zhu, Y.; Wu, G.; Song, G. Chemical grafting of nano-SiO_2 onto graphene oxide via thiol-ene click chemistry and its effect on the interfacial and mechanical properties of GO/epoxy composites. *Compos. Sci. Technol.* **2019**, *182*, 107751.

(38) Zhang, X.; Wu, Y.; Chen, X.; Wen, H.; Xiao, S. Theoretical study on decomposition mechanism of insulating epoxy resin cured by anhydride. *Polymers* **2017**, *9*, 341.

(39) Xia, Y.; Zhou, C.; Liang, G.; Gu, A.; Wang, W. Polyester-imide solventless impregnating resin and its nano-silica modified varnishes with excellent corona resistance and thermal stability. *IEEE Trans. Dielectr. Electr. Insul.* **2015**, *22*, 372−379.

(40) Zhu, M.-X.; Song, H.-G.; Li, J.-C.; Yu, Q.-C.; Chen, J.-M. Phase-field modeling of electric-thermal breakdown in polymers under alternating voltage. *IEEE Trans. Dielectr. Electr. Insul.* **2020**, *27*, 1128−1135.

(41) Xu, L.; Zhou, W.; Li, B.; Kou, Y.; Cai, H.; Chen, F.; Wang, G.; Liu, D.; Dang, Z.-M. Relaxation dynamics of Ni/epoxy composites studied by dielectric relaxation spectroscopy. *J. Elastomers Plast.* **2020**, *52*, 304−321.

(42) Wang, S.; Yu, S.; Li, J.; Li, S. Effects of functionalized nano-tio$_2$ on the molecular motion in epoxy resin-based nanocomposites. *Materials* **2020**, *13*, 163.

(43) Peddamallu, N.; Nagaraju, G.; Sridharan, K.; Velmurugan, R.; Vasa, N. J.; Nakayama, T.; Sarathi, R. Understanding the electrical, thermal, and mechanical properties of epoxy magnesium oxide nanocomposites. *IET Sci., Meas. Technol.* **2019**, *13*, 632−639.

(44) Sarathi, R.; Sahu, R. K.; Rajeshkumar, P. Understanding the thermal, mechanical and electrical properties of epoxy nanocomposites. *Mater. Sci. Eng., A* **2007**, *445−446*, 567−578.

(45) Shui, Y.; Huang, L.; Wei, C.; Chen, J.; Song, L.; Sun, G.; Lu, A.; Liu, D. Intrinsic properties of the matrix and interface of filler reinforced silicone rubber: An in situ Rheo-SANS and constitutive model study. *Compos. Commun.* **2021**, *23*, 100547.

(46) Li, H.-Y.; Li, C.-M.; Gao, J.-G.; Sun, W.-F. Ameliorated mechanical and dielectric properties of heat-resistant radome cyanate composites. *Molecules* **2020**, *25*, 3117.

(47) Shen, Z.-H.; Wang, J.-J.; Jiang, J.-Y.; Huang, S. X.; Lin, Y.-H.; Nan, C.-W.; Chen, L.-Q.; Shen, Y. Phase-field modeling and machine learning of electric-thermal-mechanical breakdown of polymer-based dielectrics. *Nat. Commun.* **2019**, *10*, 1843.

(48) Gong, Y.; Zhou, W.; Kou, Y.; Xu, L.; Wu, H.; Zhao, W. Heat conductive h-BN/CTPB/epoxy with enhanced dielectric properties for potential high-voltage applications. *High Volt.* **2017**, *2*, 172−178.

(49) Athanasopoulos, N.; Sikoutris, D.; Panidis, T.; Kostopoulos, V. Numerical investigation and experimental verification of the Joule heating effect of polyacrylonitrile-based carbon fiber tows under high vacuum conditions. *J. Compos. Mater.* **2012**, *46*, 2153−2165.

(50) Li, C.; Hu, J.; Lin, C.; He, J. The potentially neglected culprit of DC surface flashover: electron migration under temperature gradients. *Sci. Rep.* **2017**, *7*, 3271.

(51) Zhou, W.; Zhang, Y.; Wang, J.; Li, H.; Xu, W.; Li, B.; Chen, L.; Wang, Q. Lightweight porous polystyrene with high thermal conductivity by constructing 3d interconnected network of boron nitride nanosheets. *ACS Appl. Mater. Interfaces* **2020**, *12*, 46767−46778.

(52) Zhang, Z.; Yuan, L.; Liang, G.; Gu, A. Fabrication and origin of flame retarding glass fiber/bismaleimide resin composites with high thermal stability, good mechanical properties, and a low dielectric constant and loss for high frequency copper clad laminates. *RSC Adv.* **2016**, *6*, 19638−19646.

(53) Zhang, T.; Chen, X.; Zhang, Q.; Zhang, Q. M. Dielectric enhancement over a broad temperature by nanofiller at ultra-low volume content in poly(ether methyl ether urea). *Appl. Phys. Lett.* **2020**, *117*, 072905.

(54) Manikandan, T.; Siddharthan, A.; Muruganandhan, R.; Sugumaran, C. P. Influence of amine-functionalised graphene oxide filler on mechanical and insulating property of epoxy nanocomposites. *Mater. Res. Express* **2019**, *6*, 095302.

(55) Ahmed, R. M.; Ibrahiem, A. A.; El-Bayoumi, A. S.; Atta, M. M. Structural, mechanical, and dielectric properties of polyvinylchloride/graphene nano platelets composites. *Int. J. Polym. Anal. Charact.* **2021**, *26*, 68−83.

(56) Chen, M.; Zhou, W.; Zhang, J.; Chen, Q. Dielectric property and space charge behavior of polyimide/silicon nitride nanocomposite films. *Polymers* **2020**, *12*, 322.

(57) Siddabattuni, S.; Schuman, T. P.; Dogan, F. Dielectric properties of polymer-particle nanocomposites influenced by electronic nature of filler surfaces. *ACS Appl. Mater. Interfaces* **2013**, *5*, 1917−1927.

(58) Krentz, T.; Khani, M. M.; Bell, M.; Benicewicz, B. C.; Nelson, J. K.; Zhao, S.; Hillborg, H.; Schadler, L. S. Morphologically dependent alternating-current and direct-current breakdown strength in silica-polypropylene nanocomposites. *J. Appl. Polym. Sci.* **2017**, *134*, 44347.

(59) Duan, X.; Siew, W. H.; Given, M.; Liggat, J.; He, J. Effect of different surface treatment agents on the physical chemistry and electrical properties of polyethylene nano-alumina nanocomposites. *High Volt.* **2020**, *5*, 397−402.

(60) Schadler, L. S.; Chen, W.; Brinson, L. C.; Sundararaman, R.; Gupta, P.; Prabhune, P.; Iyer, A.; Wang, Y.; Shandilya, A. A perspective on the data-driven design of polymer nanodielectrics. *J. Phys. D: Appl. Phys.* **2020**, *53*, 333001.

https://doi.org/10.1021/acsomega.1c02108
ACS Omega 2021, 6, 15523−15531